LWT - Food Science and Technology 160 (2022) 113278

Contents lists available at ScienceDirect

LWT

journal homepage: www.elsevier.com/locate/lwt

Preparation and structural characterization of allicin and whey protein isolate conjugates

Hui Jiang [a,b], Zheng Xing [a,c], Mokhtar Dabbour [a,d], Benjamin Kumah Mintah [a,e], Zhaoli Zhang [a,f], Ronghai He [a,b,*], Haile Ma [a,b]

[a] School of Food and Biological Engineering, Jiangsu University, 301 Xuefu Road, Zhenjiang, Jiangsu, 212013, China
[b] Institute of Food Physical Processing, Jiangsu University, 301 Xuefu Road, Zhenjiang, Jiangsu, 212013, China
[c] School of Food Science and Technology, Huazhong Agricultural University, Wuhan, Hubei, 430072, China
[d] Department of Agricultural and Biosystems Engineering, Faculty of Agriculture, Benha University, P.O. Box 13736, Moshtohor, Qaluobia, Egypt
[e] CSIR – Food Research Institute, P. O. Box M20, Accra, Ghana
[f] School of Food Science and Engineering, Yangzhou University, 196 Huayang West Road, Yangzhou, Jiangsu, 225127, China

ARTICLE INFO

Keywords:
Allicin
Whey protein isolate
Ultrasonication
SDS-PAGE
Atomic force microscopy
Apparent viscosity

ABSTRACT

Studies have shown that the disulfide bond conjugate formed by allicin (TS) and whey protein isolate (WPI) could significantly enhance the stability of TS. Based on this, the reaction conditions of TS and WPI were optimized, and the influence of binding rate on the molecular structure, rheological properties and microstructure of the conjugates was as well examined. The results showed that the optimal conditions for the binding of TS to WPI were: temperature 25 °C, TS_{mol}: $sulfhydryl_{mol}$ = 2, pH 4, and time 30 min. With increased binding rate, surface hydrophobicity of the conjugates increased, whilst fluorescence intensity decreased. TS increased the degree of dispersion of WPI, but decreased the probability of interaction between molecules and the viscosity of the conjugates. After WPI was bound with TS, the macromolecular components decreased and the micromolecular components increased. TS-WPI conjugates were distributed in sheet-like shape, and the spherical structure of the WPI was lost. The diameter of the aggregates for 61% binding rate conjugate (following ultrasound treatment) was smaller and the distribution was more dispersed. In summary, characterization of TS-WPI conjugates could aid it applicability in the food industry, and broaden the application range of TS.

1. Introduction

Allicin (Diallyl thiosulfinate, TS) is formed under the action of Alliinase, and the reaction substrate is Alliin, a non-protein amino acid in Allium crops (namely alkyl thiocysteine and its sulfoxide compounds) (Lancaster & Collin, 1981). In intact cells, alliinase and substrates are separated, alliinine and its sulfoxide compounds are present in the cytoplasm, and alliinase is present in vacuoles. When garlic (*Allium sativum*) is crushed, there is the release of alliinase which reacts with TS, producing pyruvate, ammonia and eight thiosulfonates including TS (Whitaker, 1976).

It has long been confirmed that eating garlic can prevent or fight cancer. TS could reduce the risk of different types of tumors such as lung, stomach and colon cancer (Adewale et al., 2015). Large number of medical studies have, recently, shown that various diseases and premature aging of the human body are related to the oxidative damage of normal cells caused by excessive free radicals of oxygen in the body, and TS could regulate the incoordination of oxidative stress (Banerjee et al., 2003). Garlic is known to prevent and/or used to treat hypertension, hyperlipidemia, arteriosclerosis, inhibit platelet aggregation and anti-thrombotic formation (Abramovitz et al., 1999; Lawson et al., 2001), and could significantly reduce the content of triglyceride, low-density lipoprotein and cholesterol in serum (Ali, Al-Qattan, Al-Enezi, Khanafer, & Mustafa, 2000; Zhang et al., 2001). Although the biological activity of TS is outstanding, it has not been well utilized in practice because of the presence of thiosulfinic acid and allyl groups in the TS structure, making it sensitive to temperature and pH, and as well easily decomposed into various organic sulfur compounds (Fujisawa et al., 2008; Wang, Liu, et al., 2015). Brodnitz et al. (1971) found that pure TS was almost completely decomposed into diallyl disulfide, diallyl trisulfide, sulfur dioxide and a small amount of TS dehydration products after 20 °C for 20 h.

* Corresponding author. School of Food and Biological Engineering, Jiangsu University, 301 Xuefu Road, Zhenjiang, Jiangsu, 212013, China.
E-mail address: heronghai1971@126.com (R. He).

https://doi.org/10.1016/j.lwt.2022.113278
Received 31 August 2021; Received in revised form 15 February 2022; Accepted 20 February 2022
Available online 23 February 2022

In order to give full attention to the bioactivity of TS and increase usage, it is necessary to stabilize TS. TS stabilization technology mainly has the following four: microcapsules, liposome preparation of TS, garlic polymer micelle and TS combine with sulfhydryl substances through disulfide bond, among them, the sulfhydryl substances and TS combination method is simple, low cost, do not need high equipment.

Liang et al. (2011) indicated that the conjugates of allicin and cysteine could inhibit the proliferation of mouse colorectal cancer cells SW-480, induce apoptosis, and cause no harm to normal organs. Zhang and Parkin (2013) revealed that the conjugates of allicin and cysteine had antioxidant properties such as scavenging hydroxyl free radicals OH· and inhibiting lipid peroxidation. Chen et al. (2016) reported that the half-life of TS and soybean peptides cojugates was much higher than the pure aqueous solution of garlic. However, due to the different components of each batch of peptide prepared by enzymatic hydrolysis, the binding process of peptide and protein and the quality of the binding compound were difficult to keep stable.

Jiang et al. (2020) prepared a disulfide bond conjugates of TS and ultrasound preconditioned whey protein isolate (WPI), and observed that the mass retention rate of the conjugates after storage at different temperatures was much higher than that of TS. As a new non-thermal physical processing technology, ultrasonication has been widely used in the food industry (Chemat et al., 2011; Wang, Liu, et al., 2015). Dual-frequency ultrasound could significantly increase the content of sulfhydryl (SH) groups in the protein and improve the ability of the protein to bind TS. Compared with the unsonicated TS-WPI conjugates, the emulsifying activity and solubility of the sonicated conjugates were considerably increased by 36.35 and 24.2%, respectively (Jiang et al., 2020).

However, at present, the fundamental/technological information regarding the binding of TS and WPI, and the characterization of the conjugates with/without ultrasonication are insufficient. Therefore, the main goal of this work was to examine the structural characteristics of TS-WPI conjugates under different binding conditions. The outcome of this research can provide a theoretical foundation for the preparation of the corresponding disulfide bonds binding compound and the application of TS products.

2. Materials and methods

2.1. Materials and reagents

WPI (90% protein content) was purchased from Hillmar Co., Ltd. (Shanghai, China), and garlic was obtained from local supermarket and used directly. The reagents were acquired from Sinopharm Chemical Reagent Co., Ltd. (Beijing, China). Related/other chemicals used were of scientific grade.

2.2. Extraction and determination of TS concentration

Freshly peeled garlic was mashed and allowed to enzymatically react at 25 °C for 10 min. The resultant was mixed with distilled water in a ratio of 1:4 (W/V), and extracted at 35 °C for 1 h, then centrifuged at 4800×*g* (4 °C for 10 min) (Jiang et al., 2020). TS extract was obtained subsequent to filtration of the supernatant. The concentration of TS was quantified according to the method of Lawson et al.

2.3. Ultrasonic pretreatment of WPI solution

WPI powder was weighed and dispersed in distilled water (10 mg/mL). After stirring for 2 h (using magnetic stirrer), the solution was allowed to hydrate at 4 °C for 12 h. Afterward, the WPI solution was sonicated under the optimum sonication parameters (20 + 40 kHz, 20 min, 50 W/L, 40 °C, and the working and intermittent time ratio was 10:3) (Jiang et al., 2020).

2.4. Single factor experiment of the reaction between TS and WPI

The sulfhydryl groups in the WPI can be combined with TS, so the residual rate of the sulfhydryl groups in the WPI was used to characterize the degree of binding between the WPI and TS. Based on our preliminary experiments, the four factors of reaction including temperature, reaction time, TS to SH molar ratio (TS_{mol}:SH_{mol}) and pH value were found to have significant effect on the binding process of TS and WPI. Therefore, a single factor test was carried out under these four reaction conditions. In order to exclude the loss of sulfhydryl groups due to self-oxidation of WPI, WPI was treated under binding conditions and did not react with TS as a blank control. The residual sulfhydryl rate (*P*) and the binding rate (*R*) were calculated as follows:

$$R\,(\%) = 100 - P \tag{1}$$

$$P\,(\%) = \frac{C_1}{C_0} \times 100 \tag{2}$$

where C_0 is the protein sulfhydryl content before the reaction, μmol/g; C_1 is the protein sulfhydryl content after the reaction, μmol/g; *P* is the residual rate of the protein sulfhydryl groups, %; *R* is the binding rate of WPI and TS, %.

2.5. Preparation of TS-WPI conjugates with high and low binding rate

The molar ratio of TS to SH, pH, and reaction time have a significant impact on the binding of TS to WPI, while the molar ratio and pH can affect the structural and functional properties of the conjugates. Therefore, conjugates with high and low binding rates were prepared according to the reaction time. WPI was reacted with TS at the optimal single factor experimental conditions, and the reaction time of 30 min and 5 min was selected for the preparation of conjugates with high and low binding rate, respectively.

2.6. Molecular structure

2.6.1. Surface hydrophobicity

According to the method of Kato et al. (1995), WPI and conjugate solutions were diluted in 0.01 M phosphate buffer to 0.00125, 0.0025, 0.005, 0.01, 0.02 mg/mL. Then, 20 μL of 1-phenylaminonaphthalene-8--sulfonic acid solution was added to 4 mL of the diluted sample and mixed evenly. After reacting in the dark (at room temperature) for 15 min, the fluorescence intensity was detected at the excitation wavelength of 390 nm and emission wavelength of 471 nm (slit width of 5 nm, and scanning speed of 120 nm/min) using a spectrophotometer (Varian Inc., Palo Alto, CA, USA). The slope (hydrophobicity index) of fluorescence intensity against samples concentration was calculated with linear regression.

2.6.2. Intrinsic fluorescence spectrum

The fluorescence spectrum was examined as outlined by Huang et al. (2017) with some modification. The intrinsic fluorescence spectrum was quantified using a fluorescence spectrophotometer (Agilent Technologies Inc., Wilmington, DE, USA) at 25 ± 1 °C. WPI and conjugates solutions were excited at 295 nm and the emission wavelength was examined in the range of 280–450 nm. A constant 10 nm slit was used for excitation and emission spectra. Each scan was performed 6 times.

2.6.3. Fourier Transform infrared spectroscopy

Fourier infrared spectroscopy was performed by potassium bromide tableting method (Zhang, Wang, Dai, He, & Ma, 2018). The well-prepared samples were analysed using a Nicolet IS50 FTIR (Thermo Fisher Scientific, Waltham, MA, USA). The wave-number range was set as 4000–400 cm^{-1}. Scans (128 scans) were averaged at 4 cm^{-1} resolution, and KBr was utilized as background correction. Peakfit 4.12

software was employed for peak shape fitting and calculation of the relative percentage of secondary structure in each sample (Reich, 2005).

2.6.4. Laser confocal Raman spectroscopy

At room temperature, a DXR laser confocal Raman microscope (Thermo Fisher Scientific, Waltham, MA, USA) was used to measure the Raman spectra of WPI and conjugates. The operational parameters were set as follows: 785 nm (excitation wavelength), 300 mW (laser power), 600 gr/mm (grating), 200 nm (slit width), 600 NÅ (aperture), 2000–400 cm^{-1} (scanning range), 60 s (scanning time), 10 times of integration, and 4 times of scanning for accumulation. Raman spectral analysis software was used to calculate the relative percentage content of each disulfide bond configuration.

2.7. Zeta potential

The freeze-dried WPI and TS-WPI conjugates were mixed with distilled water to a concentration of 1 mg/mL. Zeta potential of the samples was measured using a Litesizer 500 potential analyzer (Anton Paar, Graz, Austria) at 25 °C, and the measurements were repeated 3 times (Jiang et al., 2014). Zetasizer software was applied to process and analyze the data.

2.8. Apparent viscosity

Apparent viscosity of WPI and TS-WPI conjugates (1 mg/mL in distilled water) was determined using DHR-1 rheometer (TA Instruments, Newcastle, DE, USA). The specific parameters were set as follows: temperature 25 °C, duration 120.0 s, linear mode, shear rate from 0.01 to 100.0 s^{-1} for viscosity measurement, test interval 1000 μm. The power law equation (Arancibia et al., 2011) was pplied to describe the relationship between shear rate and shear stress:

$$\tau = K\gamma\hat{n} \quad (3)$$

where τ is the shear stress, Pa; γ is the shear rate, s^{-1}; K is the viscosity constant, Pa.s; and n is the flow characteristic index, which indicates the degree of fluid deviation from Newtonian fluid.

2.9. SDS-PAGE gel electrophoresis

Sodium dodecyl sulfate-polyacrylamide gel electrophoresis (SDS-PAGE) was used to analyze the changes in the molecular weight of TS-WPI binding products with different binding rates (Laemmli, 1970). The electrode buffer was SDS-Tris-Gly solution at pH 8.3. Sample was mixed with the loading buffer in a 4:1 ratio, then heated in a water bath for 3–5 min. After cooling, 20 μL of the mixed solution and 5 μL of the marker solution were loaded into the wells and subjected to electrophoresis at 80 V in the stacking gel and 120 V in the separating gel. Gels were stained with Coomassie Brilliant Blue R-250 for 10–30 min and destained in the decolorizing solution, then scanned using Universal Hood II gel imager (Bio-Rad, Hercules, CA, USA).

2.10. Molecular weight

High performance liquid exclusion chromatography was used to determine the molecular weight (MW) (Yang et al., 2011). Waters 600 Liquid chromatography (Waters corp., Milford, MA, USA; 2487 UV detector and M32 workstation, TSKgel 3000-SWXL column: 300 × 7.8 mm) was used to characterize the MW distribution of WPI and conjugates. The samples suspensions (10 μL) were eluted at 0.5 mL/min and detected at 220 nm (30 °C).

Standards: Cytochrome C (12,500 Da), Aprotinin (6500 Da), Vitamin B12 (1355 Da), oxidized glutathione (612 Da) and glycosylglycylglycine (189 Da) were used for the calibration curve. The regression equation of the calibration curve is lg (MW) = −0.3186t + 9.4101, $R^2 = 0.9908$.

2.11. Microstructure analysis

2.11.1. Scanning electron microscopy

The freeze-dried samples were spot-coated on double-sided conductive adhesive, an electroplated layer was about 10 nm. The S–3400N scanning electron microscope (Hitachi Corp., Tokyo, Japan) was performed under an acceleration voltage of 15 kV.

2.11.2. Atomic force microscopy

Surface micro-topography was examined using the method of Guo et al. (2018). The freeze-dried samples were fully dissolved in distilled water to 100 μg/mL. Aliquots of WPI and conjugates solutions (5 μL) were rapidly dropped on a mica sheet and dried (overnight at 25 °C) in petri dishes. The microstructure and surface roughness were investigated by using Multimode 8 atomic force microscope (Bruker Inc., Billerica, MA, USA). SNL-10 B needles with elastic modulus of 0.12 n/m were selected and carried out at a scanning frequency of 1 Hz.

2.12. Statistical analysis

Results were analysed using SPSS 16.0 (IBM Corporation, USA) software under the significance level of $p < 0.05$. The graphs were drawn using Origin Pro software (IBM Inc., Chicago, IL, USA). The data were expressed as mean values (n = 3).

3. Results and discussion

3.1. Single factor result of the reaction of TS with WPI

3.1.1. Effect of temperature and time on the sulfhydryl residue rate in TS-WPI conjugates

The concentration of freshly extracted TS was 1.86 μmol/mL. The sulfhydryl content of sonicated WPI was 5 μmol/g. The residual rate of sulfhydryl groups in TS-WPI conjugates at different temperatures and times is shown in Fig. 1(a). At the first 20 min of reaction, the residual rate decreased rapidly with increasing temperature, indicating that the reaction rate and binding degree of WPI and TS increased. At 30 min, the reaction at different temperatures was basically completed and the residual rate of sulfhydryl groups was about 48%, and there was no significant difference in the degree of completion of the reaction at different temperatures. Since heat treatment will oxidize sulfhydryl groups, and even cause protein aggregation or some unnecessary side reactions, TS will be unstable at high temperatures. Therefore, the optimal reaction temperature was selected as 25 °C. Fig. 1(b) shows the sulfhydryl content of the WPI at different temperatures (not reacted with TS), which is a blank control for the reaction between WPI and TS. The loss of sulfhydryl groups caused by the oxidation of the protein itself at different temperatures was small and had no significant difference, so it could be ignored.

3.1.2. Effect of the molar ratio of SH to TS on the residual rate of sulfhydryl in TS-WPI conjugates

The influence of the molar ratio of SH to TS on the residual rate of sulfhydryl in TS-WPI conjugates is shown in Fig. 2. By increasing the amount of TS, the residual rate of sulfhydryl groups gradually decreased. At 1:2 M ratio of SH to TS, the residual rate of sulfhydryl groups was the lowest, which was 38.7% and remained stable. Thus, the molar ratio 1:2 of SH to TS was selected as the best ratio for the reaction of TS and WPI.

3.1.3. Effects of pH and time on the residual rate of sulfhydryl groups in TS-WPI conjugates

The effects of pH and time on the residual rate of sulfhydryl groups in TS-WPI conjugates are shown in Fig. 3(a). The isoelectric point of WPI was around pH 5, so the pH value of the reaction was set to 3, 4, 6, 7 and 8. The reaction, under acidic conditions, was faster than neutral and alkaline conditions. At 30 min, the reaction is almost complete (Fig. 3

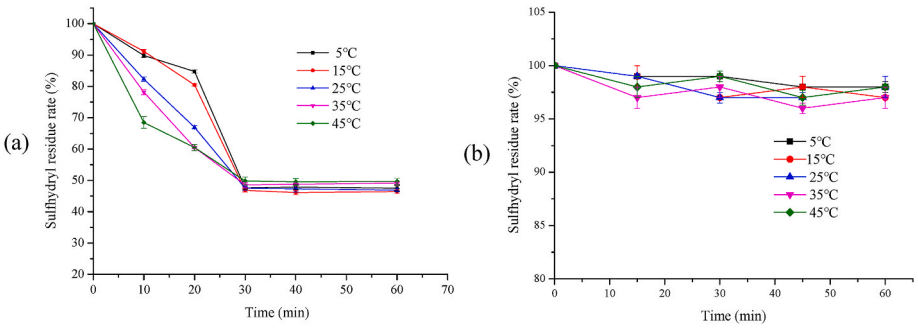

Fig. 1. Effects of temperature and time on the sulfhydryl residue rate of the TS-WPI conjugates: (a) temperature and time, (b) blank control.

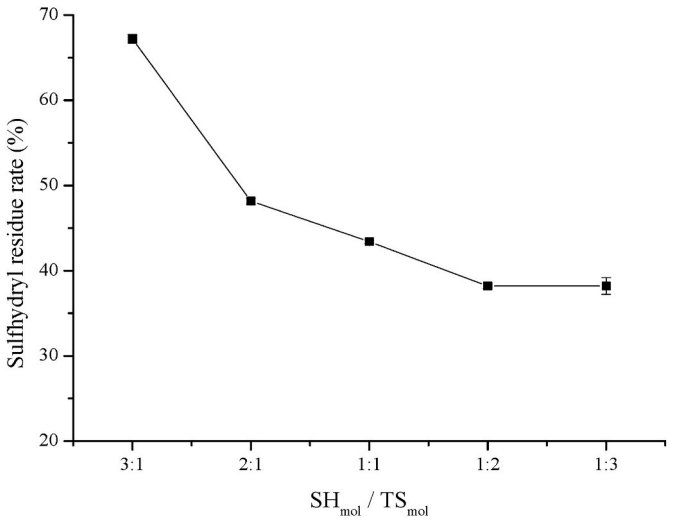

Fig. 2. Effect of the molar ratio of SH to TS on the sulfhydryl residue rate of the TS-WPI conjugates.

(a)). The residual rate of sulfhydryl groups at different pH values and at 30 min is displayed in Fig. 3(b). At pH 4, the minimum residual rate of sulfhydryl groups was 38.2% ($p < 0.05$). This may be linked to the fact that TS may have undergone hydrolysis under alkaline conditions to form diallyl disulfide, which was not conducive to the reaction. Fig. 3(c) is the blank control of the reaction, and the loss of sulfhydryl content caused by WPI self-oxidation at each pH value is negligible. In summary, the optimal conditions for the combination of TS and WPI were 25 °C, TS_{mol}:SH_{mol} = 2, pH 4, and 30 min (reaction time).

3.2. *Effect of binding rate on the molecular structure of WPI and TS-WPI conjugates*

3.2.1. *Hydrophobicity analysis*

Hydrophobicity refers to the tendency of non-polar molecular groups that are repelled by water to associate with each other in aqueous solution, which is of great significance in protein structure and conformation (Nakai, 1983; Cardamone & Puri, 1992). The surface hydrophobicity of WPI and TS-WPI conjugates is shown in Fig. 4(a). Results indicated that there was no significant difference between the hydrophobicity of sonicated and nonsonicated conjugates with the same binding rate (D and E_2 samples), and a significant difference existed between the surface hydrophobicity values at different binding rate of the conjugates ($p < 0.05$). The higher the binding rate, the greater the

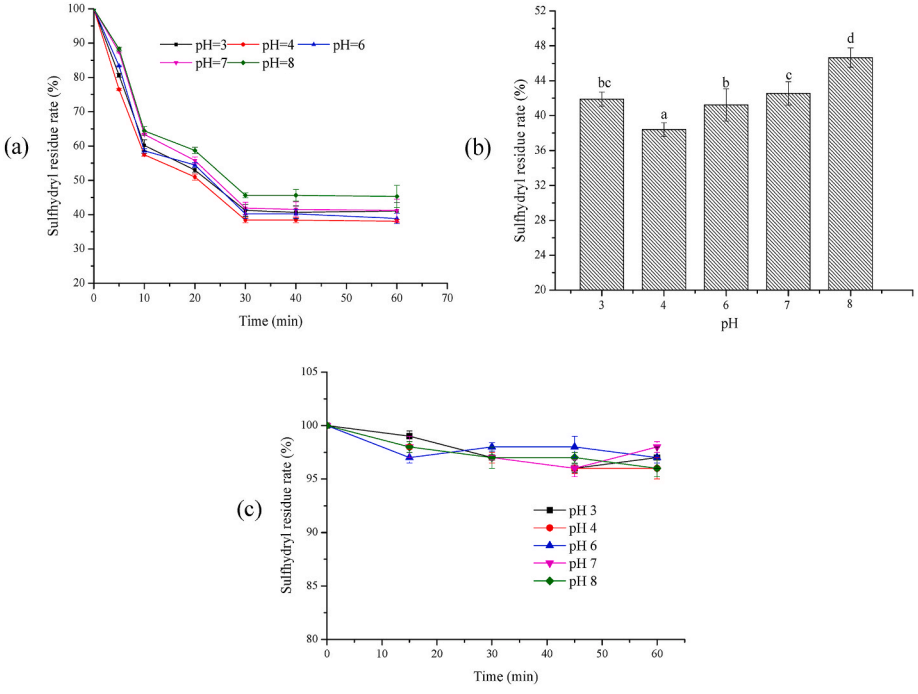

Fig. 3. Effects of pH and time on the sulfhydryl residue rate of the TS-WPI conjugates: (a) pH and time, (b) pH, (c) blank control.

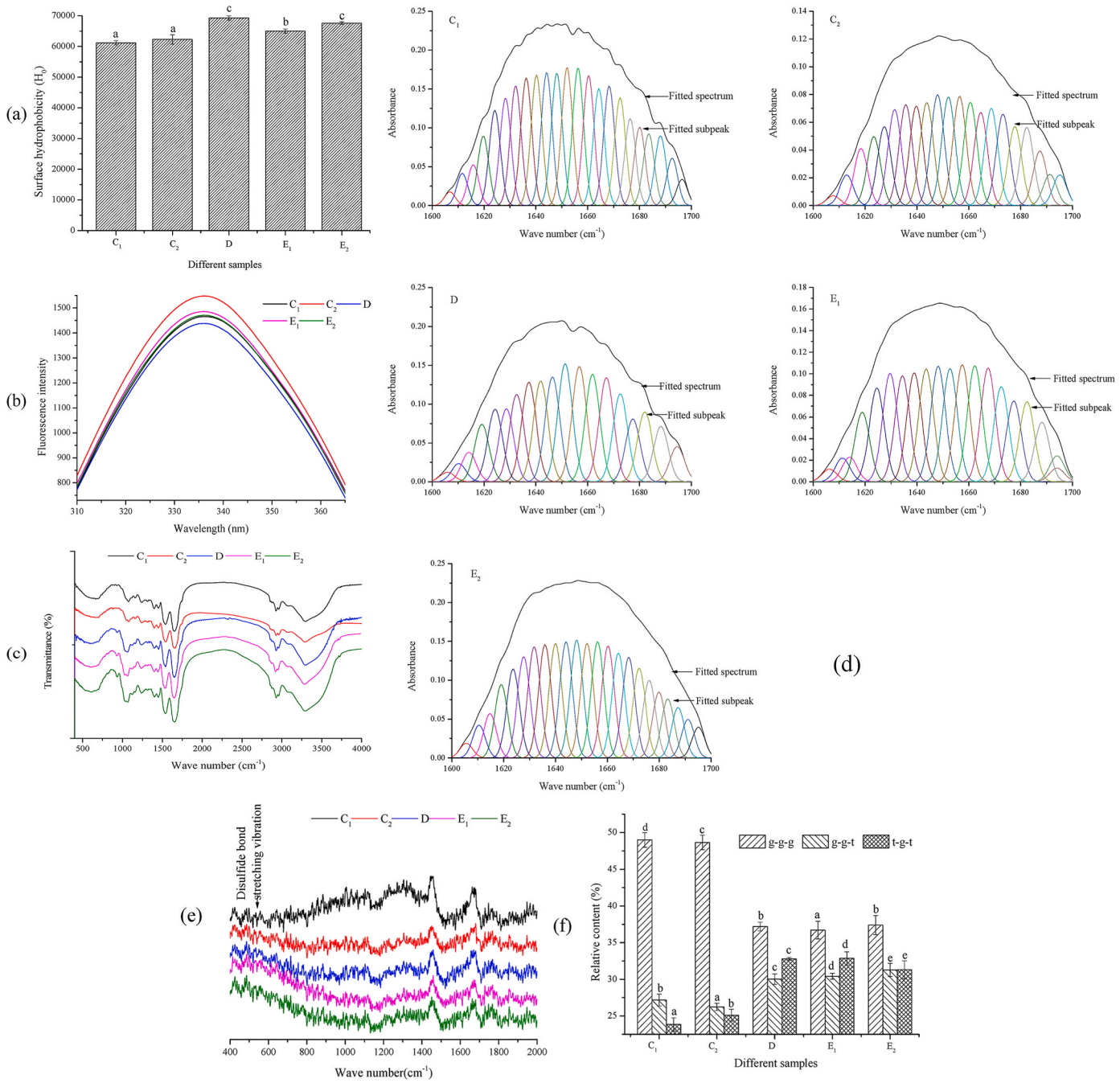

Fig. 4. Effect of binding rate on the molecular structure of WPI and TS-WPI conjugates: (a) surface hydrophobicity, (b) intrinsic fluorescence, (c) fourier infrared spectra, (d) amide band curve fitting, (e) laser Raman spectra, (f) relative content of disulfide bond configurations.

surface hydrophobicity, which was 10.66–15.93% higher than that of the unbound surface hydrophobicity. This improvement may be that the hydrophobic TS molecule could have destabilized the hydrophilic-hydrophobic balance of WPI. The increase in the number of hydrophobic groups in the WPI peptide chain increased the hydrophobicity. On the other hand, TS molecules stretched the structure of WPI molecules, and the hydrophobic groups embedded in the WPI micelles were transferred onto the surface, thereby increasing the hydrophobicity of the TS-WPI conjugates.

3.2.2. *Intrinsic fluorescence analysis*

The effect of binding rate on the intrinsic fluorescence of WPI and TS-WPI conjugates is shown in Fig. 4(b). At the excitation wavelength of 279 nm, the maximum fluorescence intensity position was detected around 336 nm, and the maximum emission wavelength was greater than 330 nm, indicating that tryptophan residues are located in the polar environment outside the molecule (Keerati-U-Rai, Miriani, Iametti, Bonomi, & Corredig, 2012). The order of fluorescence intensity was: $C_2 > E_1 > E_2 > C_1 > D$. The fluorescence intensity of the sonicated WPI was higher than that of the untreated sample. This may be due to the unfolding of the spatial structure of the WPI following ultrasonication, and the tryptophan residues inside the protein were exposed at the surface of the molecule, thus showing a stronger fluorescence intensity. After WPI was bound with TS, the fluorescence intensity decreased, and the higher the binding rate, the more obvious the decrease in fluorescence intensity. The curling and folding of WPI may have also caused the chromophore to be exposed to the solvent, resulting in a decrease in fluorescence intensity.

3.2.3. Fourier infrared spectral analysis

The spectra of WPI and TS-WPI conjugates are shown in Fig. 4(c). The amide I region (1700–1600 cm^{-1}) is most sensitive to changes in protein conformation, so it is usually used for the analysis of protein secondary structure (Ramos et al., 2013; Zhang, Zhang, Lin, & Vardhanabhuti, 2012). The fractions of secondary structure were examined at wavenumber: 1660–1651 cm^{-1}, α-helix; 1639–1600 cm^{-1}, β-sheet; 1700–1661 cm^{-1}, β-turn; and 1650–1640 cm^{-1}, random coil. Compared with WPI, the absorption peak of WPI in the amide I band following sonication did not change significantly, while the absorption peak of the conjugates was significantly enhanced.

The curve fitting spectrum (1700–1600 cm^{-1}) was performed using the second derivative spectrum and deconvolution technique in OMNIC and PeakFit software, as shown in Fig. 4(d). The relative content of the secondary structure of the sample is presented in Table 1. The hydrogen bond is the main force for stabilizing the secondary structure, the α-helix of protein is usually inside the polypeptide chain and is a tightly bound spatial structure (Hopp, 1986). After ultrasonic treatment, the α-helix of WPI decreased and the random coil increased significantly ($p < 0.05$). This indicated that ultrasonic treatment could change the environment of amino acids and affect the hydrogen bonds in the protein structure, altering the protein structure from ordered to disordered. When TS was combined with WPI, α-helix decreased and β-sheet increased, indicating that the structure of WPI was stretched. TS increased the steric hindrance of WPI, which increased the random coil structure of the conjugates. As the binding rate increased, the random coil increased, and the structure changed from order to disorder.

3.2.4. Laser Raman spectroscopy analysis

In order to compare the differences between the disulfide bond configuration of WPI and conjugates, as proof of the occurrence of the binding reaction, laser Raman spectroscopy was performed. The Raman shifts of disulfide bonds in different vibration modes were different. Fig. 4(e) shows the spectra of WPI and TS-WPI conjugates in the wavenumber of 2000–400 cm^{-1}. At 510–500 cm^{-1} is gauche-gauche-gauche (g-g-g) mode, 525–515 cm^{-1} is gauche-gauche-trans (g-g-t) mode, and 545–535 cm^{-1} is *trans*-gauche-trans (t-g-t) mode. The g-g-g is the main configuration of the disulfide bonds in WPI (Fig. 4(f)). This finding was similar with the observation of Przulj et al. (2004), that the g-g-g configuration in the disulfide bonds of native soybean protein isolate was the largest. After ultrasonic treatment, the relative content of g-g-g and g-g-t configuration in WPI disulfide bonds decreased, and the relative content of t-g-t configuration increased. Following combination of WPI with TS, the relative content of various configurations of different conjugates was changed. By comparing the conjugates (D, E_1, E_2) with C_1 and C_2, the relative content of the g-g-g configuration decreased, but the relative content of the other configurations (g-g-t and t-g-t) increased ($p < 0.05$). This observation indicated that the combination with TS altered the disulfide bond configuration of WPI, and TS had a greater impact on the change in disulfide bonds configuration of WPI than sonication. The higher the combination rate, the more the relative content of the g-g-g configuration, and the less the relative content of the t-g-t configuration ($p < 0.05$). These results demonstrated that the enhancement of H_0 may be related to the increase in the relative content of g-g-t and t-g-t configurations. The reason may be that the g-g-g configuration in the disulfide bonds could hinder the exposure of hydrophobic groups.

Table 1
Secondary structure content (%) of WPI and TS-WPI conjugates.

Samples	α-helix	β-sheet	β-turn	Random coil
WPI	19.0 ± 0.5 ^{c}	35.0 ± 2.4 ^{b}	34.0 ± 2.3 ^{a}	11.6 ± 0.5 ^{a}
WPI (ultrasonic)	16.4 ± 1.0 ^{b}	26.2 ± 1.1 ^{a}	40.3 ± 3.4 ^{b}	23.1 ± 0.7 ^{d}
Binding rate 61%	16.6 ± 1.5^{b}	37.7 ± 0.9 ^{b}	31.1 ± 2.7 ^{a}	14.6 ± 1.3 ^{b}
Binding rate 38% (ultrasonic)	15.5 ± 0.8 ^{b}	37.4 ± 2.5 ^{b}	32.7 ± 1.9 ^{a}	14.4 ± 1.4 ^{b}
Binding rate 61% (ultrasonic)	13.1 ± 1.2 ^{a}	36.8 ± 1.8 ^{b}	32.7 ± 2.8 ^{a}	17.4 ± 1.7 ^{c}

3.3. Zeta potential analysis

The effect of binding rate on zeta potential of WPI and TS-WPI conjugates is shown in Fig. 5. The zeta potential of different samples was negative, as the binding rate increased, the absolute value of zeta potential decreased gradually. Wong et al. found that the zeta potential increased with decreased pH value, and the zeta potential was approximately zero at the isoelectric point of WPI (pH 5.0) (Wong et al., 2011). However, TS may affect the electrostatic and hydrophobic interactions of the WPI dispersion system, leading to zeta potential of the TS-WPI conjugates less than zero. Moreover, the pH is the most important factor affecting the zeta potential of the dispersion system, therefore, the zeta potential of conjugates (pH 4.0) was higher than that of the WPI solution (pH 7.0).

3.4. Apparent viscosity analysis

The apparent viscosity curves of different samples are shown in Fig. 6. The viscosity of the sample decreased as the shear rate increased, which was called shear thinning (Hu et al., 2013). When the shear rate was lower than 10 s^{-1}, as the shear rate increased, the apparent viscosity decreased rapidly. This could possibly be linked to the orientation effect of molecules and particles caused by the increase in shear rate, which was much higher than the random motion effect caused by brown effect. When the shear rate gradually increased, the shear thinning behavior became weaker and weaker. After reaching a certain rate, it exhibited properties similar to the newtonian fluid (Malhotra & Coupland, 2004). The viscosity of sonicated WPI was significantly higher than that of untreated sample. This may be associated with the unfolding and changes of the WPI structure, causing an improvement in the hydrodynamic radius of the protein, which enhanced the interaction with water, then increased the viscosity of the solution. The conjugates of TS and WPI had a smaller viscosity than the sonicated WPI. This may be due to the increase in the degree of dispersion of the conjugates molecules and the decrease in the probability of interaction between the molecules, inducing a reduction in viscosity.

Table 2 presents the relevant parameters of the rheological curve

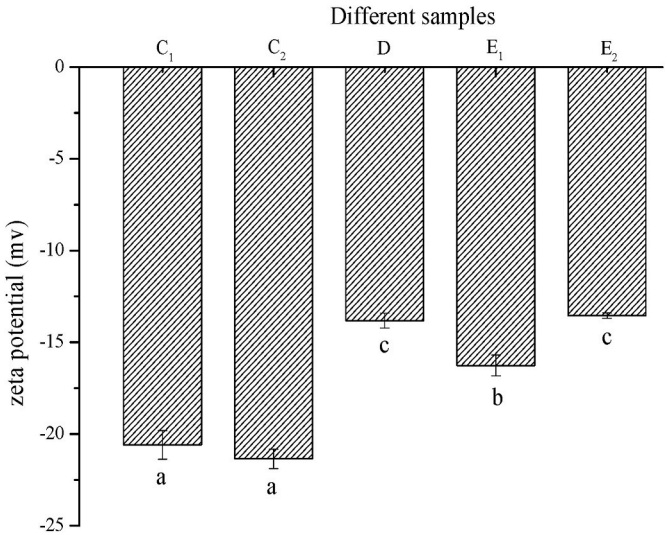

Fig. 5. Effect of binding rate on zeta potential of WPI and TS-WPI conjugates.

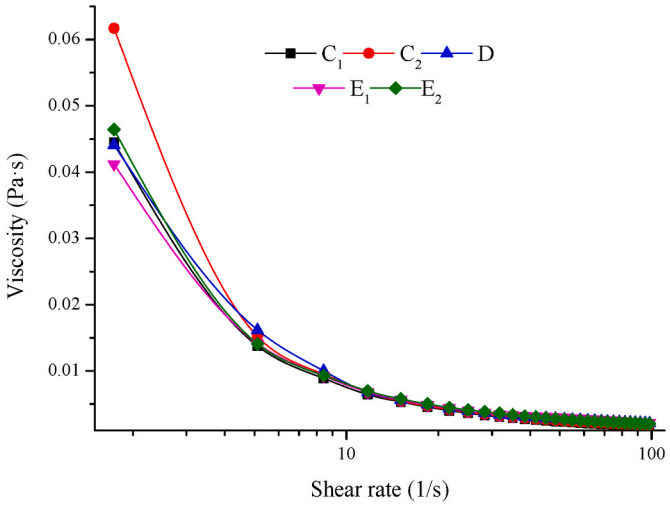

Fig. 6. Effect of binding rate on apparent viscosity of WPI and TS-WPI conjugates.

fitted with the power law model $\tau = K\gamma\hat{}n$. There was no significant difference between the viscosity coefficients of WPI and TS-WPI conjugates ($p > 0.05$). Furthermore, the highest value of n was obtained for the conjugate E_1, suggesting that the conjugate E_1 was the most obvious non-Newtonian fluid properties. Ultrasonic pretreatment and TS caused changes in the values of the rheological characteristic index (n) of the WPI solution. These changes could be associated with the alteration in the structure of the WPI or the interaction between the WPI and TS.

3.5. SDS-PAGE gel electrophoresis analysis

Fig. 7 shows the electrophoretogram of the WPI and TS-WPI conjugates. WPI was characterized with five distinct bands, from top to bottom, which were immunoglobulin (Ig G), lactoferrin (Lf), serum albumin (BSA), β-lactoglobulin (β-Lg), and α-lactoglobulin (α-La). The bands and mobility of the electrophoretic spectrum of sonicated WPI were similar to that of unsonicated WPI, demonstrating that the distribution of WPI composition and molecular weight did not change significantly after ultrasonic treatment. These findings suggested that the primary structure of the protein was not destroyed. Moreover, TS-WPI conjugates resulted in slight differences in molecular-weight/bands compared with WPI, α-La, β-Lg had slightly narrow band. The reason was that coomassie brilliant blue could combine with sulfhydryl on protein through electrostatic non-covalent bonds to form a color reaction. After the reaction of WPI and TS, the content of sulfhydryl of WPI decreased, which reduced the binding with coomassie brilliant blue. In addition, after 1 mol SH reacted with TS, the molecular weight increased by 72 Da only, so the molecular weight of the conjugates did not significantly increase. No changes were observed in the protein bands of the samples with different binding rates due to the changes in the molecular weight of the WPI caused by the differences in binding rates could not be reflected in the electrophoretogram.

Table 2
Changes of n value, K value and correlation coefficient R^2 in the rheological curve fitted by the power law model.

Samples	Rheological characteristic index n	Viscosity coefficient K (Pa·s)	R^2
WPI	0.4164 ± 0.04 [a]	0.0211 ± 0.008 [a]	0.9794 ± 0.07
WPI (ultrasonic)	0.4611 ± 0.03 [ab]	0.0236 ± 0.005 [a]	0.9754 ± 0.08
Binding rate 61%	0.5120 ± 0.04 [b]	0.0190 ± 0.001 [a]	0.9866 ± 1.00
Binding rate 38% (ultrasonic)	0.5426 ± 0.07 [b]	0.0178 ± 0.0015 [a]	0.9904 ± 0.06
Binding rate 61% (ultrasonic)	0.4660 ± 0.03 [ab]	0.0210 ± 0.003 [a]	0.9898 ± 0.04

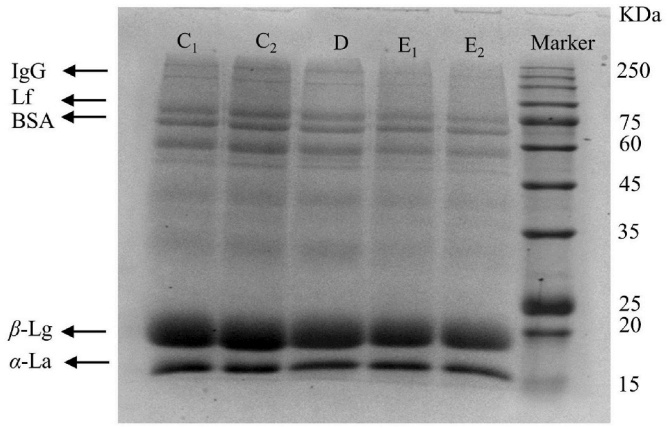

Fig. 7. Effect of binding rate on SDS-PAGE of WPI and TS-WPI conjugates.

3.6. Molecular weight analysis

High performance liquid exclusion chromatography was used to further verify the change in molecular weight of WPI after the combination with TS. Fig. 8 shows the molecular weight (chromatogram) of WPI and TS-WPI conjugates,and the molecular weight distribution of the conjugates is presented in Table 3. Following ultrasonic treatment of WPI, ultrasonic cavitation destroyed some aggregates with molecular weight greater than 1000 kDa, and the relative content of this fraction (1000 kDa) was significantly reduced by 51.8%, while the relative content of those below 20 kDa increased by 8%. After WPI was bound with TS, the relative content of molecular weight greater than 1000 kDa decreased by 80.0–88.3% ($p < 0.05$), but the relative content of less than 20 kDa fraction increased by 23.5–27.7%. There was no significant difference in the molecular weight distribution of conjugates with different binding rates.

3.7. Microstructure analysis

3.7.1. Scanning electron microscopy

Scanning electron microscope images of WPI and TS-WPI conjugates are shown in Fig. 9(a). WPI had a typical spherical structure of globulin. This structure varies in size and the surface was relatively smooth. After ultrasonic treatment, the structure of WPI was broken and became loose, and there were obvious depressions in the middle of the spherical structure. This was due to the violent shearing action, cavitation effect and thermal effect on WPI by the ultrasonic wave (Wali et al., 2017). After WPI was bound with TS, the surface became smoother and distributed in a flaky shape. This observation may be due to the covalent bonding of WPI and TS, the molecules were fully stretched, resulting in the loss of the spherical structure of WPI and the formation of new structure and microscopic state.

3.7.2. Atomic force microscope

Fig. 9(b) shows the atomic force microscopy images of WPI and TS-WPI conjugates. The unsonicated WPI particles were large and had viscious agglomeration. After ultrasonic treatment, the WPI aggregates begun to loosen and became finely dispersed on the surface of the mica sheet, but the size of WPI particles was not uniform. The diameter of the aggregates in the sonicated conjugate (61% binding rate) was smaller and the distribution was more dispersed.

The surface roughness of the sample represents the overall level of the surface micro-topography and is a quantitative indicator of the

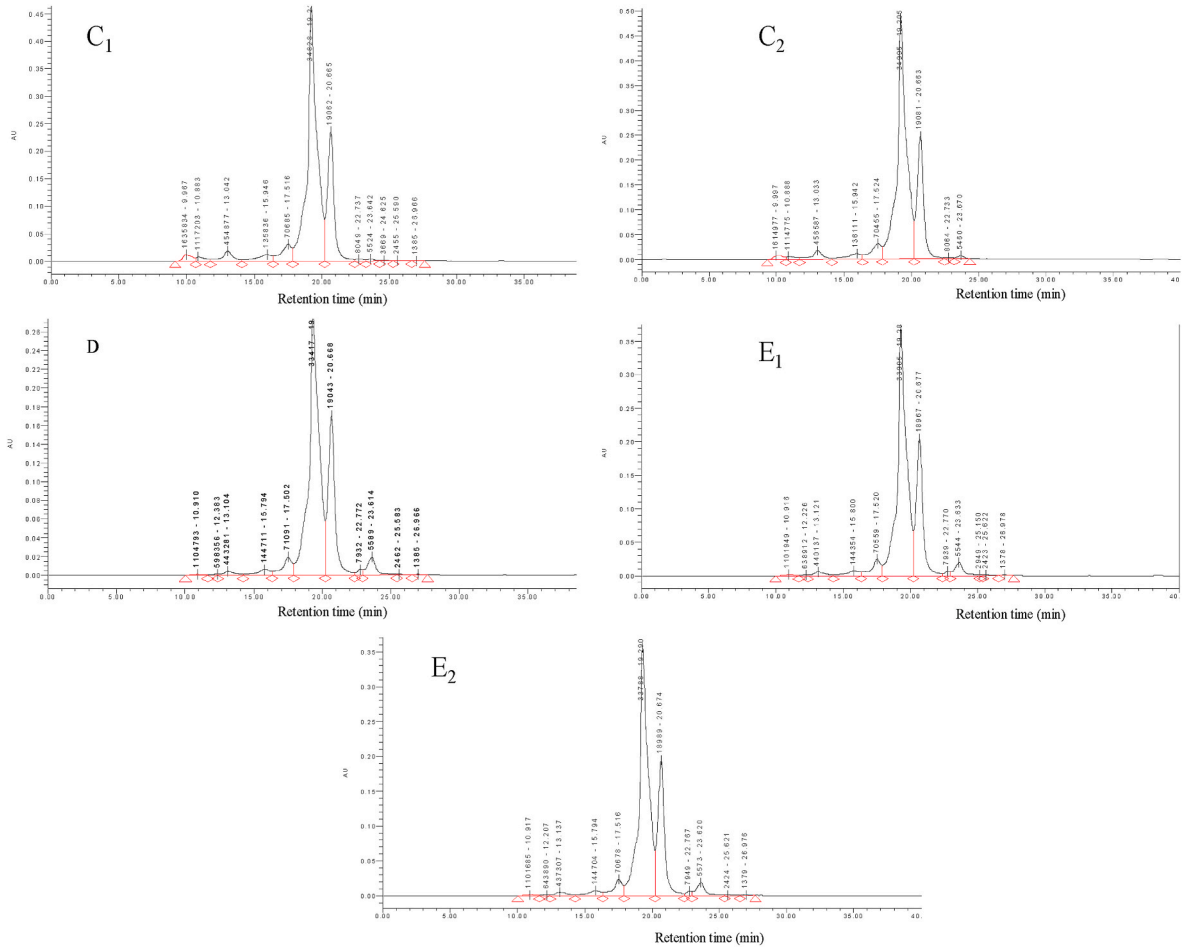

Fig. 8. Molecular weight chromatogram of WPI and TS-WPI conjugates.

Table 3
Molecular weight distribution of WPI and TS-WPI conjugates.

Molecular weight distribution (kDa)	The content of different samples (%)				
	WPI	WPI (ultrasonic)	Binding rate 61%	Binding rate 38% (ultrasonic)	Binding rate 61% (ultrasonic)
1000	1.97 ± 0.08 [b]	0.95 ± 0.05 [b]	0.19 ± 0.05 [a]	0.28 ± 0.04 [a]	0.23 ± 0.03 [a]
100–1000	5.24 ± 0.19 [b]	5.34 ± 0.45 [b]	2.89 ± 0.22 [a]	3.12 ± 0.30 [a]	3.20 ± 0.10 [a]
40–100	4.62 ± 5.04 [a]	4.67 ± 1.58 [a]	4.05 ± 1.73 [a]	4.13 ± 2.05 [a]	4.14 ± 1.22 [a]
20–40	64.11 ± 2.02 [a]	63.08 ± 3.15 [a]	62.05 ± 2.47 [a]	62.66 ± 1.55 [a]	62.68 ± 1.68 [a]
1–20	24.13 ± 1.35 [a]	26.06 ± 1.30 [a]	30.81 ± 1.80 [b]	29.81 ± 1.10 [b]	29.75 ± 0.89 [b]
Sum	100	100	100	100	100

micro-topography. The apparent roughness Ra (average roughness) and Rq (root mean square of the roughness Z value) of the samples are displayed in Table 4. The results showed that the Ra and Rq of WPI were 2.96 nm and 1.67 nm, respectively. The surface roughness of sonicated WPI changed significantly, which increased by 6.76% and 13.77% respectively ($p < 0.05$). The roughness of the surface of WPI could affect the binding reaction with TS, when the surface roughness of the WPI increased, and the larger the surface area that reacted with TS, the more favorable the reaction was. After WPI was combined with TS, the roughness of unsonicated and sonicated TS-WPI conjugates decreased significantly ($p < 0.05$).

4. Conclusions

In this study, the optimal condition for the reaction of TS with WPI was obtained, and the structural characteristics of conjugates with different binding rates were analysed. The surface hydrophobicity and fluorescence analysis indicated that the higher the binding rate of the conjugate, the greater the surface hydrophobicity of the conjugates, and the more obvious the fluorescence intensity was reduced. With the increase in binding rate the random coil increased, and the structure changed from order to disorder. Raman spectroscopy demonstrated that the disulfide bond configuration of WPI changed after it was bound with TS, and the g-g-g configuration in the disulfide bonds hindered the exposure of hydrophobic groups. The viscosity of conjugates decreased compared to the WPI, and the binding rate of 61% (without ultrasonic pretreatment) showed the most significant non-newtonian fluid characteristics. Compared with WPI, the microstructure of TS-WPI conjugates changed, and the roughness of the conjugate decreased significantly.

Credit author statement

I have made substantial contributions to the conception, design of the work, the acquisition, analysis, and interpretation of data for the work. I have drafted the work and revised it critically for important

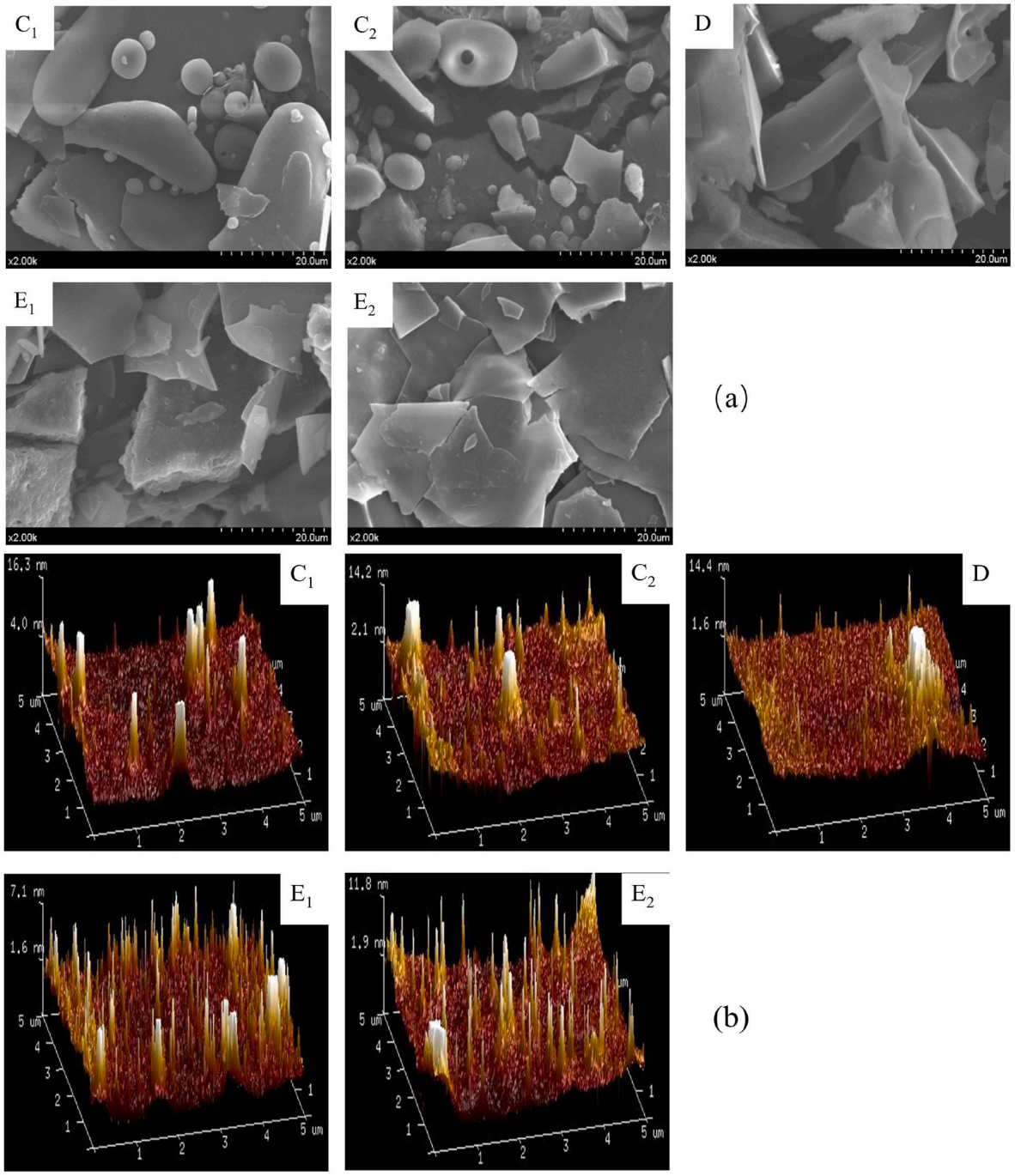

Fig. 9. Microstructure diagram of WPI and TS-WPI conjugates: (a) scanning electron microscope images, (b) atomic force microscopy images.

Table 4
Surface roughness of WPI and TS-WPI conjugates.

Samples	WPI	WPI (ultrasonic)	Binding rate 61%	Binding rate 38% (ultrasonic)	Binding rate 61% (ultrasonic)
R_a (nm)	2.96 ^{d}	3.16 ^{e}	2.83 ^{c}	2.15 ^{a}	2.31 ^{b}
R_q (nm)	1.69 ^{c}	1.9 ^{d}	1.60 ^{b}	1.62 ^{b}	1.5 ^{a}

intellectual content. I have approved the final version to be published. I agree to be accountable for all aspects of the work in ensuring that questions related to the accuracy or integrity of any part of the work are appropriately investigated and resolved. No conflict of interest exits in the submission of this manuscript, and manuscript is approved by all authors for publication. I would like to declare on behalf of my co-authors that the work described was original research that has not been published previously, and not under consideration for publication elsewhere, in whole or in part. All the authors listed have approved the manuscript that is enclosed.

Declaration of competing interest

The authors declare that they have no known competing financial interests or personal relationships that could have appeared to influence the work reported in this paper.

Acknowledgments

This work was sponsored by Primary Research & Development Plan of Jiangsu Province (BE2017308, BE2018311) and Jiangsu Agricultural Science and Technology Innovation Fund (CX (18) 3038), sponsored by a project Funded by the Priority Academic Program Development of Jiangsu Higher Education Institutions (PAPD).

References

Abramovitz, D., Gavri, S., Harats, D., Levkovitz, H., Mirelman, D., Miron, T., et al. (1999). Allicin-induced decrease in formation of fatty streaks (atherosclerosis) in mice fed a cholesterol-rich diet. *Coronary Artery Disease, 10*(7), 515–519.

Adewale, O., Brimson, J., Odunola, O., Gbadegesin, M., Owumi, S., Isidoro, C., et al. (2015). The potential for plant derivatives against acrylamide neurotoxicity. *Phytotherapy Research, 29*(7), 978–985.

Ali, M., Al-Qattan, K., Al-Enezi, F., Khanafer, R., & Mustafa, T. (2000). Effect of allicin from garlic powder on serum lipids and blood pressure in rats fed with a high cholesterol diet. *Prostaglandins Leukotrienes and Essential Fatty Acids, 62*(4), 253–259.

Arancibia, C., Jublot, L., Costell, E., & Bayarri, S. (2011). Flavor release and sensory characteristics of o/w emulsions. Influence of composition, microstructure and rheological behavior. *Food Research International, 44*(6), 1632–1641.

Banerjee, S., Mukherjee, P., & Maulik, S. (2003). Garlic as an antioxidant: The good, the bad and the ugly. *Phytotherapy Research, 17*(2), 97–106.

Brodnitz, M., Pascale, J., & Derslice, L. (1971). Flavor components of garlic extract. *Journal of Agricultural and Food Chemistry, 19*(2), 273–275.

Cardamone, M., & Puri, N. (1992). Spectrofluorimetric assessment of the surface hydrophobicity of proteins. *Biochemical Journal, 282*(2), 589–593.

Chemat, F., Huma, Z., & Khan, M. (2011). Applications of ultrasound in food technology: Processing, preservation and extraction. *Ultrasonics Sonochemistry, 18*(4), 813–835.

Chen, H., Zhang, C., & Hua, Y. (2016). Preparation and characterization of disulfide bonds of allicin and soybean protein source sulfhydryl peptides. *Food and Fermentation Industry, 42*(8), 75–80.

Fujisawa, H., Suma, K., Origuchi, K., Seki, T., & Ariga, T. (2008). Thermostability of allicin determined by chemical and biological assays. *Journal of the Agricultural Chemical Society of Japan, 72*(11), 2877–2883.

Guo, X., Sun, X., Zhang, Y., Wang, R., & Yan, X. (2018). Interactions between soy protein hydrolyzates and wheat proteins in noodle making dough. *Food Chemistry, 245*(15), 500–507.

Hopp, T. P. (1986). Protein surface analysis. Methods for identifying antigenic determinants and other interaction sites. *Journal of Immunological Methods, 88*(1), 1–18.

Huang, L., Ding, X., Dai, C., & Ma, H. (2017). Changes in the structure and dissociation of soybean protein isolate induced by ultrasound-assisted acid pretreatment. *Food Chemistry, 232*, 727–732.

Hu, H., Wu, J., Li-Chan, E., Zhu, L., Zhang, F., Xu, X., et al. (2013). Effects of ultrasound on structural and physical properties of soy protein isolate (SPI) dispersions. *Food Hydrocolloids, 30*(2), 647–655.

Jiang, L., Wang, J., Li, Y., Wang, Z., Liang, J., Wang, R., et al. (2014). Effects of ultrasound on the structure and physical properties of black bean protein isolates. *Food Research International, 62*, 595–601.

Jiang, H., Xing, Z., Wang, Y., Zhang, Z., Mintah, B., Dabbour, M., et al. (2020). Preparation of allicin-whey protein isolate conjugates: Allicin extraction by water, conjugates' ultrasound-assisted binding and its stability, solubility and emulsibility analysis. *Ultrasonics Sonochemistry, 63*, 104981.

Kato, Y., Aoki, T., Kato, N., Nakamura, R., & Matsuda, T. (1995). Modification of ovalbumin with glucose 6-phosphate by amino-carbonyl reaction. Improvement of protein heat stability and emulsifying activity. *Journal of Agricultural and Food Chemistry, 43*(2), 301–305.

Keerati-U-Rai, M., Miriani, M., Iametti, S., Bonomi, F., & Corredig, M. (2012). Structural changes of soy proteins at the oil–water interface studied by fluorescence spectroscopy. *Colloids and Surfaces B: Biointerfaces, 93*, 41–48.

Laemmli, U. K. (1970). Cleavage of structural proteins during the assembly of the head of *bacteriophage T4*. *Nature, 227*(5259), 680–685.

Lancaster, J. E., & Collin, H. A. (1981). Presence of alliinase in isolated vacuoles and of alkyl cysteine sulphoxides in the cytoplasm of bulbs of onion. *Plant Science Letters, 22*(2), 169–176.

Lawson, L., Wang, Z., & Papadimitriou, D. (2001). Allicin release under simulated gastrointestinal conditions from garlic powder tablets employed in clinical trials on serum cholesterol. *Planta Medica, 67*(1), 13–18.

Liang, D., Qin, Y., Zhao, W., Zhai, X., Guo, Z., Wang, R., et al. (2011). S-allylmercaptocysteine effectively inhibits the proliferation of colorectal cancer cells under *in vitro* and *in vivo* conditions. *Cancer Letters, 310*(1), 69–76.

Malhotra, A., & Coupland, J. (2004). The effect of surfactants on the solubility, zeta potential, and viscosity of soy protein isolates. *Food Hydrocolloids, 18*(1), 101–108.

Nakai, S. (1983). Structure-function relationships of food proteins: With an emphasis on the importance of protein hydrophobicity. *Journal of Agricultural and Food Chemistry, 31*(4), 676–683.

Przulj, N., Wigle, D., & Jurisica, I. (2004). Functional topology in a network of protein interactions. *Bioinformatics, 20*(3), 340–348.

Ramos, S., Reinas, I., Silva, S., Fernandes, J., Cerqueira, M., Pereira, R., et al. (2013). Effect of whey protein purity and glycerol content upon physical properties of edible films manufactured therefrom. *Food Hydrocolloids, 30*(1), 110–122.

Reich, G. (2005). Near-infrared spectroscopy and imaging: Basic principles and pharmaceutical applications. *Advanced Drug Delivery Reviews, 57*(8), 1109–1143.

Wali, A., Ma, H., Aadil, R., Zhou, C., Rashid, M., & Liu, X. (2017). Effects of multifrequency ultrasound pretreatment on the enzymolysis, ACE inhibitory activity, and the structure characterization of rapeseed protein. *Journal of Food Processing and Preservation, 41*(6), 13413.

Wang, H., Li, X., Liu, X., Shen, D., Qiu, Y., Zhang, X., et al. (2015). Influence of pH, concentration and light on stability of allicin in garlic (*Allium sativum* L.) aqueous extract as measured by UPLC. *Journal of the Science of Food and Agriculture, 95*(9), 1838–1844.

Wang, T., Liu, F., Wang, R., Wang, L., Zhang, H., & Chen, Z. (2015). Solubilization by freezemilling of water-insoluble subunits in rice proteins. *Food & Function, 6*(2), 423–430.

Whitaker, J. R. (1976). Development of flavor, odor, and pungency in onion and garlic. *Advances in Food Research, 22*, 73–133.

Wong, B., Day, L., & Augustin, M. (2011). Deamidated wheat protein–dextran Maillard conjugates: Effect of size and location of polysaccharide conjugated on steric stabilization of emulsions at acidic pH. *Food Hydrocolloids, 25*(6), 1424–1432.

Yang, B., Yang, H., Li, J., Li, Z., & Jiang, Y. (2011). Amino acid composition, molecular weight distribution and antioxidant activity of protein hydrolysates of soy sauce lees. *Food Chemistry, 124*(2), 551–555.

Zhang, G., & Parkin, K. (2013). A tissue homogenate method to prepare gram-scale allium thiosulfinates and their disulfide conjugates with cysteine and glutathione. *Journal of Agricultural and Food Chemistry, 61*(12), 3030–3038.

Zhang, X., Derek, L., Paul, G., Stephen, F., Connock, M., & Maslin, D. (2001). Gender may affect the action of garlic oil on plasma cholesterol and glucose levels of normal subjects. *The Journal of Nutrition, 131*(5), 1471–1478.

Zhang, S., Zhang, Z., Lin, M., & Vardhanabhuti, B. (2012). Raman spectroscopic characterization of structural changes in heated whey protein isolate upon soluble complex formation with pectin at near neutral pH. *Journal of Agricultural and Food Chemistry, 60*(48), 12029–12035.

Zhang, Z., Wang, Y., Dai, C., He, R., & Ma, H. (2018). Alkali extraction of rice residue protein isolates: Effects of alkali treatment conditions on lysinoalanine formation and structural characterization of lysinoalanine-containing protein. *Food Chemistry, 261*, 176–183.